A New Methodology for Ultra-Fast and Accurate Statistical EMT Analysis in Electric Power-Systems

Luis A. Garcia-Reyes*, J. R. Zuluaga and J. L. Naredo

Abstract – This paper introduces Quadrature Mirror Filter Electromagnetic Transient (QMF-EMT) methodology as a novel, precise, and ultra-fast method for statistical studies (SS) of EMTs in electrical networks. Building on a previously proposed approach for real-time EMT simulation, QMF-EMT incorporates nonlinear elements such as surge arresters, sequential switching operations, and a statistical switching model. The method is highly parallelizable and achieves superior accuracy and computational speed compared to conventional time-domain (TD) and frequency-domain (FD) techniques. The effectiveness of QMF-EMT is demonstrated through its application to the statistical analysis of two test networks. Validation is performed by comparing the results with established techniques, including PSCAD/EMTDC and the Numerical Laplace Transform (NLT) method. The case studies include the integration of surge arresters, controlled switching operations as overvoltage (OV) mitigation measures, and a large-scale network comprising 39 three-phase nodes. Notably, QMF-EMT's high computational speed on conventional CPUs enables efficient determination of the required number of events and integration steps for statistical analyses. This work underscores QMF-EMT's potential as a transformative tool for addressing computational challenges in EMT studies, particularly in large-scale power-systems.

Keywords – electromagnetic switching transients, statistical analysis, insulation coordination, Kron reduction, frequency domain synthesis, nonlinear elements.

I. Introduction

THE coordination of insulation design, expansion, and operation of power-systems typically requires extensive SS of their responses to EMTs. The primary objective of these studies is to achieve technically and economically viable solutions, often involving thousands of simulations of the same electrical network [1]-[5]. Simulations can be executed in the TD using EMTP-type programs [6] on conventional CPUs, whose operation is essentially sequential and demands excessive computation time and resources from personnel assigned to the studies [7]-[12]. As a result, analysts may be compelled to conduct a reduced number of simulations at low resolutions; that is, they must use large integration steps. This scenario is undesirable as it does not guarantee the attainment of appropriate technical and economic solutions.

Moreover, there are no clear criteria for selecting the number of simulations or the appropriate integration step size for each study involving statistical analysis of EMTs in power-systems. Some experts recommend simulating between 100 and 300 scenarios [13], while others consider 500 simulations are necessary [4], [5]. A recent study suggested performing up to 3000 simulations for adequate insulation design [2]. Regarding the integration step size, a commonly recommended value is $\Delta t = 25\mu s$ for switching and fault transients, considering a maximum significant frequency of 20 kHz [14]. However, this article demonstrates that this value may not be the most suitable for SS. Additionally, a limitation of EMTP-type programs utilizing ULM-type line models [15] is that the integration step must be at least ten times smaller than the propagation time for the shortest transmission line in the power-system under study. Therefore, the presence of lines shorter than 75 km requires integration steps smaller than $25\mu s$.

One strategy to reduce time and costs in SS involves dividing the network under analysis into two parts: one, typically with fewer nodes, is designated as the primary area of interest, while the other is considered the external or secondary area of interest [13]. Detailed modeling of the primary area is then conducted using simplified or rational equivalent network models for the secondary area [16]. However, it has been demonstrated that the use of simplified models in the external area can significantly affect the accuracy of the studies [3], and rational equivalent network models based on infinite impulse response (IIR) filters are often subject to passivity issues [16], [17]. To avoid these issues, finite impulse response (FIR) convolutions can be used.

Another methodology to accelerate EMT simulations is to use parallel and multi-rate computing, as described in references [18]-[21]. These techniques can be implemented on conventional CPUs; however, achieving higher performance may require massively parallel computing hardware, which entails higher costs. Moreover, the associated programming techniques are highly specialized.

An alternative to TD methods are FD techniques, such as the NLT [22]-[25], which has recently been applied to the statistical analysis of EMTs, offering a substantial reduction in simulation times [3]. However, a major drawback of conventional NLT-based methods is that simulations involving successive switch operations require two Laplace transformations—one direct and one inverse—per operation, which significantly increases simulation time and error accumulation.

Therefore, the primary objective of this paper is to present a methodology for conducting SS of EMTs in power-systems with ultra-fast and accurate performance computing massively FIR convolutions. This approach is designed to run efficiently on conventional CPU hardware, reducing reliance on

This work was supported in part by the National Council of Science and Technology (CONACYT), Mexico, under Grant No. 1074592. The work of Luis A. Garcia-Reyes received funding from the ADOreD project, part of the European Union's Horizon Europe Research and Innovation Programme, under the Marie Skłodowska-Curie Grant Agreement No. 101073554.

L. A. Garcia-Reyes is with Centre d'Innovació Tecnològica en Convertidors Estàtics i Accionaments, Universitat Politècnica de Catalunya (CITCEA-UPC), BCN 08028 ESP (e-mail of corresponding author: luis.reyes@upc.edu). J. R. Zuluaga is with Intel Corporation, GDL 45017 MEX (jean.zuluaga.duque@intel.com). J. L. Naredo is with Center for Research and Advanced Studies of the National Polytechnic Institute (Cinvestav-IPN), Guadalajara Unit, GDL 45019 MEX (luis.naredo@cinvestav.mx).

Paper submitted to the International Conference on Power Systems Transients (IPST2025) in Guadalajara, Mexico, June 8-12, 2025.

specialized large-scale parallel computing infrastructure. The simulation algorithm is based on the QMF-EMT method proposed in [26]. The algorithm synthesizes a reduced system model in the Laplace domain, bypassing rational equivalents, and performs simulations in TD, avoiding the overhead of double Laplace transformations for each switch operation. This method enables a high volume of simulations with smaller time steps, providing faster and more precise SS for large-scale power-systems compared to conventional methodologies. Furthermore, the identification of appropriate time steps and the number of simulations contributes to addressing the lack of criteria for selecting these crucial simulation parameters.

The paper is organized as follows: Section II describes the algorithm developed for simulating EMTs in power-systems, including nonlinearities. Section III presents a 17-node 3-phase network with switch operations and surge arresters. These cases are also simulated using PSCAD/EMTDC and the conventional NLT method [3], [22]-[25]. Section IV discusses considerations for statistical switch operations. Section V details SS-EMTs on the same 17-node network, demonstrating that the method's efficiency allows variation in simulation count and resolution to adequate study parameters. It also compares two OV mitigation techniques—controlled switching operations and surge arresters—to determine the most effective approach. Section VI presents SS-EMT results, showing that the proposed methodology achieves computational efficiency independent of network size, relying instead on the number of nodes of interest.

II. SIMULATION OF NETWORKS IN TIME-DOMAIN

The transient calculation methodology employed in this work is based on the nodal representation of an electrical system in the Laplace domain, expressed as:

$$\mathbf{I}(\mathrm{s}) = \mathbf{Y}(\mathrm{s})\mathbf{V}(\mathrm{s})\,, \tag{1}$$

where $\mathrm{s} = c + j\omega$ is the Laplace variable, with ω representing the angular frequency and c being a real, finite constant. $\mathbf{I}(\mathrm{s})$ and $\mathbf{V}(\mathrm{s})$ are the vectors of nodal currents and voltages, respectively. $\mathbf{Y}(\mathrm{s})$ is the admittance matrix of the network and can be categorized into the following three groups:

1) Nodes of interest: Connected to switches and subjected to transient disturbances.
2) Energized nodes: Connected to steady-state sources.
3) Nodes of no interest: Not energized and not requiring observation.

Nodes in group 3 can be eliminated through a Kron reduction by partitioning the system under study as follows:

$$\begin{bmatrix}\mathbf{I}_1(\mathrm{s})\\ \mathbf{I}_2(\mathrm{s})\end{bmatrix} = \begin{bmatrix}\mathbf{Y}_{11}(\mathrm{s}) & \mathbf{Y}_{12}(\mathrm{s})\\ \mathbf{Y}_{21}(\mathrm{s}) & \mathbf{Y}_{22}(\mathrm{s})\end{bmatrix}\begin{bmatrix}\mathbf{V}_1(\mathrm{s})\\ \mathbf{V}_2(\mathrm{s})\end{bmatrix}, \tag{2}$$

where $\mathbf{Y}_{11}(\mathrm{s})$, $\mathbf{I}_1(\mathrm{s})$ and $\mathbf{V}_1(\mathrm{s})$ represent the submatrix of admittances, the sub-vector of injected currents, and the vector of nodal voltages, respectively, corresponding to groups 1 and 2 of nodes described above. $\mathbf{Y}_{22}(\mathrm{s})$, $\mathbf{I}_2(\mathrm{s})$ and $\mathbf{V}_2(\mathrm{s})$ are the respective terms corresponding to group 3. $\mathbf{Y}_{12}(\mathrm{s})$ and $\mathbf{Y}_{21}(\mathrm{s}) = \boldsymbol{Y}_{12}^{T}$ are the mutual admittance submatrices between nodes of groups 1-2 and 3. Thus, we have:

$$\mathbf{I}_1(\mathrm{s}) = \mathbf{Y}_{\mathrm{red}}(\mathrm{s})\mathbf{V}_1(\mathrm{s}) + \mathbf{Y}_{12}(\mathrm{s})\mathbf{Y}_{22}^{-1}(\mathrm{s})\mathbf{I}_2(\mathrm{s})\,, \tag{3}$$

$$\mathbf{Y}_{red}(\mathrm{s}) = \mathbf{Y}_{11}(\mathrm{s}) - \mathbf{Y}_{12}(\mathrm{s})\mathbf{Y}_{22}^{-1}(\mathrm{s})\mathbf{Y}_{21}(\mathrm{s})\,. \tag{4}$$

By rearranging equation (3) to solve for $\mathbf{V}_1(\mathrm{s})$:

$$\mathbf{V}_1(\mathrm{s}) = \mathbf{Z}_{red}(\mathrm{s})\mathbf{I}_1(\mathrm{s}) + \mathbf{Z}_{SS}(\mathrm{s})\mathbf{I}_2(\mathrm{s})\,, \tag{5}$$

with:

$$\mathbf{Z}_{red}(\mathrm{s}) = \mathbf{Y}_{red}^{-1}(\mathrm{s})\,, \tag{6a}$$

$$\mathbf{Z}_{ss}(\mathrm{s}) = -\mathbf{Z}_{red}(\mathrm{s})\mathbf{Y}_{12}(\mathrm{s})\mathbf{Y}_{22}^{-1}(\mathrm{s})\,. \tag{6b}$$

The second term on the right-hand side of equation (5) represents the contributions of steady-state sources to the overall response of the power-system, while the first term corresponds to contributions from auxiliary sources representing transient disturbances. Since these disturbances are modeled using simple switch operations, instead of the matrix-vector multiplication for this term, it is replaced with the following scalar multiplication of a vector [26]:

$$\mathbf{Z}_{red}(\mathrm{s})\mathbf{I}_1(\mathrm{s}) = \boldsymbol{\mathcal{Z}}(\mathrm{s})I_{sw}(s), \tag{7}$$

where the vector $\boldsymbol{\mathcal{Z}}(\mathrm{s})$ results from subtracting the two columns of $\mathbf{Z}_{\boldsymbol{red}}(\mathrm{s})$ corresponding to the connection nodes of the active switch, and $I_{sw}(s)$ is the current from the auxiliary source representing that switch. Substituting (7) into (5) yields:

$$\mathbf{V}_1(\mathrm{s}) = \boldsymbol{\mathcal{Z}}(\mathrm{s})\, I_{sw}(s) + \mathbf{Z}_{SS}(\mathrm{s})\, \mathbf{I}_2(s). \tag{8}$$

Expression (8) is now implemented sequentially to simulate disturbances involving "p" simple switch operations. Since the simulation begins at steady-state, equation (8) becomes:

$$\mathbf{V}_1^{(0)}(\mathrm{s}) = \mathbf{Z}_{SS}(\mathrm{s})\mathbf{I}_2(s_0), \tag{9}$$

where the superscript "$^{(0)}$" indicates that no transient event has yet occurred. After the occurrence of the first and subsequent events, expression (8) takes the following form:

$$\begin{aligned}\mathbf{V}_1^{(p)}(\mathrm{s}) = {} & \boldsymbol{\mathcal{Z}}^{(p)}(\mathrm{s})\, I_{sw}^{(p)}(s) + \mathbf{V}_1^{(p-1)}(\mathrm{s})\\ & + \Delta Z_{red}^{(p)}(\mathrm{s}_0)\, \mathbf{I_2}(\mathrm{s}_0),\end{aligned} \tag{10}$$

where p=1, 2, 3, …P. Considering that:

$$\Delta Z_{red}^{(p)}(\mathrm{s}_0) = Z_{red}^{(p)}(\mathrm{s}_0) - Z_{red}^{(p-1)}(\mathrm{s}_0). \tag{11}$$

It is noteworthy that the matrix $\boldsymbol{Z}_{ss}(s)$ depends on $\boldsymbol{Z}_{red}(s)$ as shown in equation (6b). However, between transient events, it is only necessary to evaluate the contribution made by the change in impedance $\Delta Z_{red}^{(p)}(\mathrm{s}_0)$, which is a small modification that will only affect the steady-state frequency of the sources. This means that, unlike $\boldsymbol{Z}_{red}(s)$, $\Delta Z_{red}^{(p)}$ can be treated as a difference impedance vector at frequency (s_0).

Finally, expressions (10) and (11) are transformed into the discrete TD. For the right-side expression in (8), which corresponds to the steady-state voltage, we have:

$$\boldsymbol{v}_1^{(0)}(n) = \mathcal{L}_N^{-1}\{\boldsymbol{Z}_{ss}\mathbf{I}_2(\mathrm{s}_0)\} = \boldsymbol{v}_{1,SS}(n), \tag{12}$$

where $\mathcal{L}_N^{-1}\{\,\}$ represents the numerical inverse Laplace transform (INLT), although $\boldsymbol{v}_{1,SS}(n)$ is actually obtained using phasor methods. For expression (10), we obtain:

$$\boldsymbol{v}_1^{(p)}(n) = \boldsymbol{\zeta}^{(p)}(n) * i_{sw}^{(p)}(n) + \boldsymbol{v}_1^{(p-1)}(n) + \boldsymbol{v}_{\text{phasor}}^{(p)}, \quad (13)$$

where the operator "$*$" represents convolution, and:

$$\boldsymbol{\zeta}^{(p)}(n) = \mathcal{L}_N^{-1}\{\boldsymbol{Z}^{(p)}(\mathrm{s})\}, \quad (14)$$

with:

$$\boldsymbol{v}_{\text{phasor}}^{(p)} = \left|\Delta Z_{red}^{(p)}(\mathrm{s}_0)\mathbf{I}_{\mathbf{2}}(\mathrm{s}_0)\right| cos\left(\omega t + \angle\left(\Delta Z_{red}^{(p)}(\mathrm{s}_0)\mathbf{I}_{\mathbf{2}}(\mathrm{s}_0)\right)\right). \quad (15)$$

It should be noted that neither (12) nor (15) requires the INLT, as this expression merely represents a phasor. For simulating a transient disturbance involving "p" simple switch operations, equations (13) and (15) are applied recursively.

It can be observed that for a network with a three-phase switch, there are 2^3 possible combinations of $\Delta Z_{red}^{(p)}$, which could be computationally expensive. However, the Kron reduction significantly reduces this computational cost. Furthermore, for each iteration "p" in equation (11), while it is not possible to predict the state, it is feasible to calculate all the possible combinations in advance and have them readily available for each iteration. Each iteration "p" can be computed in parallel, and, by applying the QMF-EMT methodology [26], all convolutions can also be parallelized. In this approach, parallelism is leveraged twice: by convolving each impulse response of $\boldsymbol{\zeta}^{(p)}(n)$ in parallel, and by applying the QMF-EMT procedure to $\boldsymbol{\zeta}^{(p)}(n)$.

A. Sequential operation of the switch

The simulation begins with the network voltages in steady-state as indicated in (12), and subsequently, the operations are executed sequentially as shown in equation (13). The equivalent Norton source required by the switch model is given by the voltage difference between nodes *j* and *k* [24]:

$$i_{sw}^{(p)}(n) = \begin{cases} -\left[\left(v_j^{(p)}(n) - v_k^{(p)}(n)\right)u(n-\tau_c)\right]/R_{sw}; \text{ close} \\ \left[\left(v_j^{(p)}(n) - v_k^{(p)}(n)\right)u(n-\tau_o)\right]/R_{sw}; \text{ open} \end{cases} \quad (16)$$

where τ_c and τ_o are the effective closing and opening times, respectively; $u(n)$ is the unit step function, and R_{sw} is the equivalent Norton resistance of the switch, typically set to 1 $m\Omega$. Similarly, the matrix $\Delta Z_{red}^{(p)}(\mathrm{s}_0)$ also changes with each switch operation; however, this last term is only affected at the steady-state frequency of the excitation source.

B. Nonlinear elements

For the simulation of nonlinear elements such as surge arresters, the piecewise-linear approximation method is employed through sequential switching operations following the technique detailed in [22]-[24]. Nonlinear characteristics are typically represented in *v-i* or *f-i* tables or graphs, as shown in Fig. 1, where the nonlinear behavior is approximated using *M* linear segments with slopes R_{xM}. Each segment represents an equivalent that the network sees toward the nonlinear element within its corresponding operating zone [22]. This is illustrated in Fig. 2 for a surge arrester connected between nodes *j* and *k*. The voltage across these nodes, denoted as $V_{nonlin}(\mathrm{s})$, is given by the following linear relation within its corresponding operating zone:

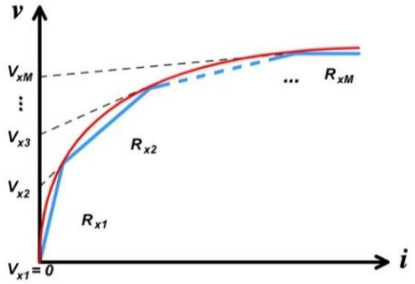

Fig. 1. Nonlinear curve approximation using *M* linear segments.

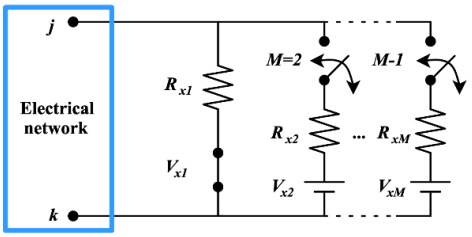

Fig. 2. Model of a surge arrester represented by *M* linear segments.

$$V_{nonlin}(\mathrm{s}) = V_{xM} + \left[\,\mathrm{Y}_{j,k}(\mathrm{s}) + 1/R_{xM}\,\right]^{-1} I_{nonlin}(\mathrm{s})\,. \quad (17)$$

Applying the inverse Laplace transform to (17) leads to an iterative TD solution, analogous to (13), expressed as:

$$v_{nonlin}(n) = V_{xM} + \zeta_{j,k}(n) * i_{nonlin}(n)\,, \quad (18)$$

$$\zeta_{j,k}(n) = \mathcal{L}_N^{-1}\left\{\left[\,\mathrm{Y}_{j,k}(\mathrm{s}) + 1/R_{xM}\,\right]^{-1}\right\}. \quad (19)$$

Here, $\mathrm{Y}_{j,k}(\mathrm{s})$ represents the admittance at the connection point of the surge arrester. By modifying (6a) for each of the *M*-th sections of the arrester, its nonlinear behavior is represented sequentially. Notice that introducing M linear segments requires the sequential closings and openings of switches $1, 2, 3, \ldots M$. The auxiliary Norton current source is given by:

$$i_{nonlin}(n) = \begin{cases} -[(v_{nonlin}(n) - v_{xM})u(n-\tau_{nlc})]/R_{xM} \\ [(v_{nonlin}(n) - v_{xM})u(n-\tau_{nlo})]/R_{xM} \end{cases}, \quad (20)$$

where τ_{nlc} is the time when $v_{nonlin}(n)$ exceeds v_{xM}; τ_{nlo} is when $v_{nonlin}(n)$ is less than v_{xM} and, R_{xM} and v_{xM} are the equivalent resistance and transition voltage that contain the *M*-th operating zone of the nonlinear element [22], defined as:

$$R_{xM} = \frac{R_{M-1}R_M}{R_{M-1} - R_M}\,, \quad (21)$$

$$v_{xM} = \frac{R_{M-1}v_M - v_{M-1}R_M}{R_{M-1} - R_M}\,. \quad (22)$$

It follows from equation (18) that the proposed approach eliminates the need for repeated time-frequency and frequency-time transformations (NLT and INLT, respectively) across each operating zone, offering a significant advantage over conventional FD-based methods such as those in [22]-[24]. This feature substantially reduces computational costs and minimizes the accumulation of errors typically introduced by multiple NLT operations. Accordingly, only the initial INLT computations are retained, as indicated in equation (19).

III. QMF-EMT METHODOLOGY VALIDATION

To assess the QMF-EMT method, it is applied to the simulation of transient events in the 17-node three-phase AC-60 Hz system shown in Fig. 3. The transient responses are first obtained using the conventional NLT technique [3], [22]-[25], followed by PSCAD/EMTDC v. 4.6.3, and finally, the QMF-EMT method. In all cases, the simulation time is 60 ms and the time step is $\Delta t = 7.32\ \mu s$. This results in $N = 2^{13} = 8192$ samples. With this number of samples, the NLT can be tuned to an overall accuracy of 10^{-8} [22]-[24]. Due to this accuracy, the NLT is adopted here as the reference to evaluate the precision of the other two methods. The simulations with PSCAD/EMTDC have also been run with time steps $\Delta t = 0.732\ \mu s$ and $\Delta t = 0.1464\ \mu s$. This is to corroborate that reducing the time step in PSCAD/EMTDC brings its results closer to those of the NLT.

The parameters for the network in Fig. 3 are taken from [26]. In the PSCAD/EMTDC simulations, all transmission lines are represented using the Universal Line Model (ULM), whereas in both the NLT and QMF-EMT methods, the lines are modeled using their AB frequency-dependent nodal matrices [25]. All simulations were conducted on a 2.7 GHz Intel i5 PC with 8 GB of RAM using MATLAB R2022b.

A. Sequential closure (case 1)

Consider that the network in Fig. 3 is initially energized and in steady-state, with the three-phase circuit breaker CB_1 (between buses 4 and C) in the open position. At times 27.0, 29.9, and 32.6 ms, the CB_1 poles close sequentially in an ABC sequence. The resulting voltage waveforms at bus C are obtained using the conventional NLT, PSCAD/EMTDC, and QMF-EMT methods, and they are plotted in Fig. 4. Note the close agreement among the three sets of plots, which validates the QMF-EMT method being proposed. By taking the NLT results as a reference, it can be established that the ones from the QMF-EMT method present an overall accuracy of 0.01%, while the ones from PSCAD/EMTDC present an overall accuracy of 1.0%. The computation times for this simulation are 11.631 s for the proposed method, 16.673 s for the NLT, and 30.583 s for PSCAD/EMTDC. It should be noted that these times include the model buildup (i.e., preprocessing). The accuracy of PSCAD/EMTDC can be improved up to 0.1% by reducing the time step. Time step reduction to $\Delta t = 0.732\ \mu s$ will increase the computation time to 174.59 s.

B. Sequential opening (case 1)

Consider now that CB_1 between buses 4 and C has been closed for a sufficiently long time to attain its steady-state; then the CB_1 poles open in ABC sequence at times 16.7 ms, 19.7 ms and 22.7 ms. Note that these times do not necessarily correspond to the zero-crossings of the associated currents. The inclusion of zero-crossing considerations is straightforward. Fig. 5 presents the voltage waveforms resulting from this maneuver as obtained with NLT, PSCAD/EMTDC and QMF-EMT. Both, the accuracies and the computing times remain essentially equal to those in previous case.

It is worth noting the better accuracy of QMF-EMT with respect to NLT at the very first and very last samples. This result is attributed here to the fact that, unlike the NLT technique, QMF-EMT does not require the back-and-forth NLT conversions that contribute to error accumulation in the conventional NLT method.

C. Sequential closure with surge arresters (case 2)

Consider again, as in case III.A, that CB_1 is open; however, now CB_2 at bus D is also open and remains so throughout the 60 ms simulation time. Now, the poles of CB_1 close in ABC sequence at times 8.9, 10.3, and 13.3 ms. This time, a surge arrester has been added at bus D (see case 2 detail in Fig. 3).

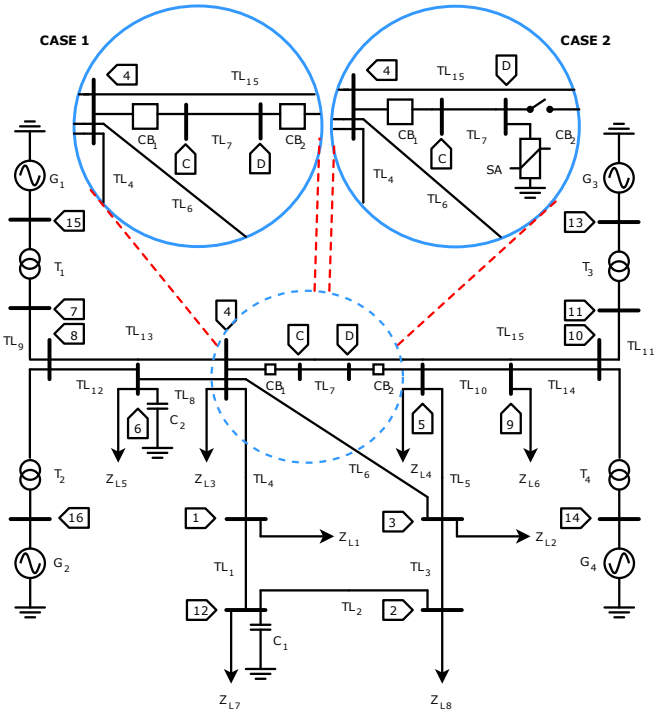

Fig. 3. 17-node three-phase test network, with detail on the two test cases.

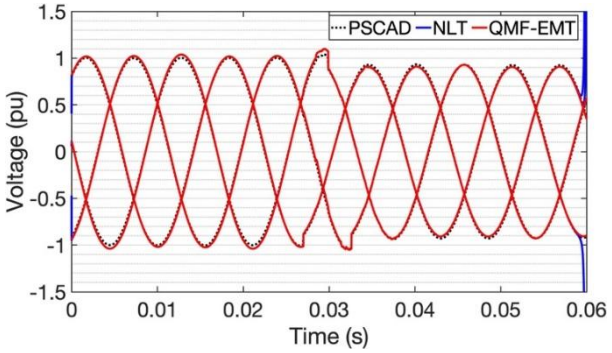

Fig. 4. Closing voltages at node *C*.

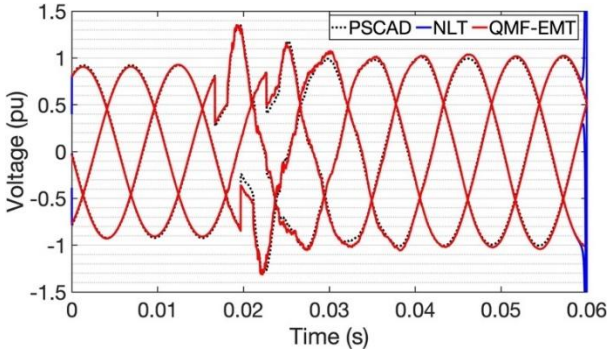

Fig. 5. Opening voltages at node *C*.

TABLE I
CHARACTERISTICS $v - i$ OF THE SURGE ARRESTER.

Voltage (pu)	Current (kA)	Voltage (pu)	Current (kA)
1.2	0.000471	1.4	0.00250
1.3	0.000745	1.5	0.01340

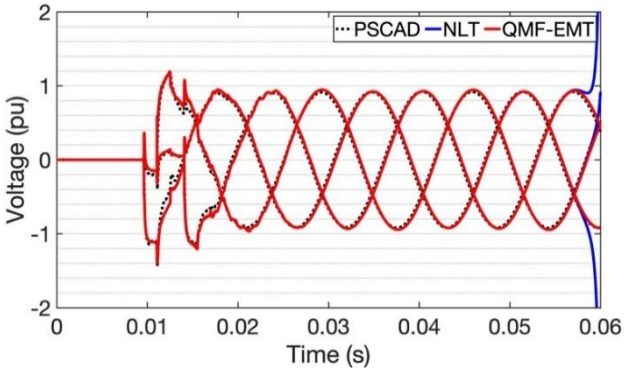

(a) With surge arresters.

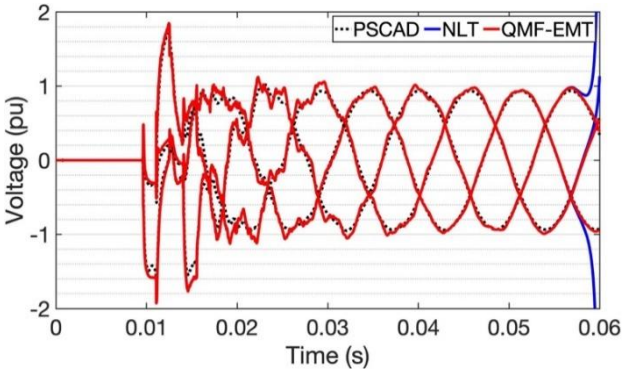

(b) Without surge arresters.

Fig. 6. Closing voltages at node *D*.

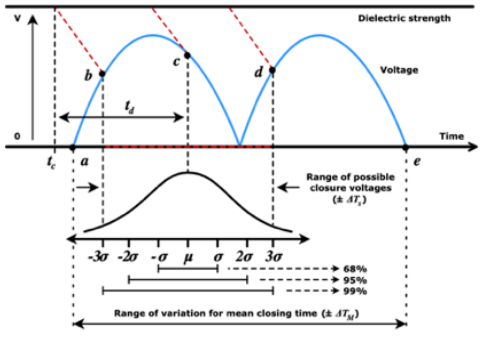

(a) Switch closing.

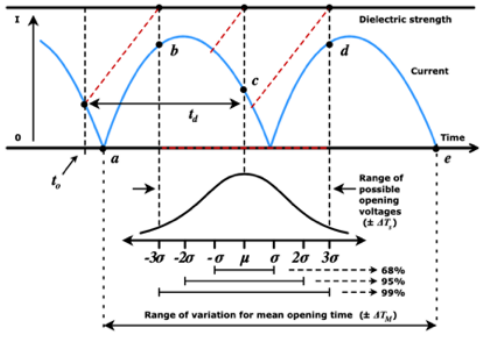

(b) Switch opening.

Fig. 7. Statistical operation scheme of the switch.

The *v-i* characteristics of the surge arrester are given in Table I. The voltage waveforms resulting from the closings at bus D, as obtained with conventional NLT, PSCAD/EMTDC, and QMF-EMT, are plotted in Fig. 6a. For comparison purposes, the same waveform plots without the surge arrester are provided in Fig. 6b. The computation times are 14.231 s for the proposed method, 30.767 s for the conventional NLT, and 32.429 s for PSCAD/EMTDC.

QMF-EMT is thus 56% faster than PSCAD/EMTDC and 53% faster than the conventional NLT. As for the accuracies of QMF-EMT and PSCAD/EMTDC compared to the conventional NLT, these remain the same as in case 1.

IV. STATISTICAL MODEL OF THE SWITCH

For a statistical study, the operation time T_{op} of the switch consists of three terms. First, there is the mean time ΔT_M which should vary over a given time period by a uniform distribution (typically one cycle of the fundamental frequency). Second, there is the time accounting for the dispersion of the effective closing or opening time ΔT_s, which should be statistically represented, typically by a normal or Gaussian distribution [2],[3]. Third, there is the defined time t_d which depends on and includes the operating characteristics and conditions of the switch and may or may not include the delay between the emission and reception of the control signal by the device (typically 3.7 ms) [4]. Therefore, T_{op} is given by:

$$T_{op} = \Delta T_s + \Delta T_M + t_d \,, \tag{23}$$

Figs. 7a and 7b illustrate the statistical functioning scheme of the switch, for both closures and openings. In this scheme, it is assumed that the dielectric resistance is the same for both negative and positive half-cycles.

The ideal moment for closing or opening is assumed to be at point *c*, which considers a uniform variation from point *a* to point *e*. Between points *b* and *d* the dispersion of the contacts is considered with a normal distribution and depends on the operating speed of the switch. It is recommended to consider a dispersion in the range $[-3\sigma, 3\sigma]$, as this probability is close to 99.73%, which implies covering the majority of cases [1].

A. Controlled operation of the switch

This process involves operating each phase switch at the optimal waveform point to minimize OVs. For closures, the signal ensures action near the voltage waveform's zero-crossing, while for openings, it aligns with the current's zero-crossing [27]. As a result, events occur sequentially for a three-phase switch, with phase operating times detailed in [2].

B. Operation of the switch with surge arresters

When surge arresters are used to control OVs, the circuit breaker trip command is typically simultaneous, with switch operations occurring at the same time, as noted in [2]. However, each pole maintains its own statistical dispersion.

V. STATISTICAL STUDIES

The proposed QMF-EMT method is applied to various switch opening scenarios using the test network in Fig. 3, with

a $\Delta t = 12.21\ \mu s$, an accurate time step derived by halving the typical recommended value of $25\ \mu s$. This value follows the common practice in discrete FD analysis, based on a sample count that is a power of two. The switch operates within 50 to 67 ms (one cycle), utilizing the previously established statistical model and the technical specifications outlined in [28]. The simulation time used was 60 ms.

A. Case 1: Varying the number of simulations

A SS of OV openings was conducted for 10, 100, 1000 and 10000 simulations without OV control, using Matlab R2022b environment. EMTs responses at node C were evaluated, with probability distribution (PD) and accumulative probability (AP) displayed in Figs. 8 and 9. Results indicate that 1000 simulations suffice: increasing from 100 to 1000 (Figs. 8b and 8c) significantly changes the OV-PD, while increasing to 10000 (Fig. 8d) merely refines histogram resolution (as seen in Fig. 9). Thus, the proposed method enables accurate SS with 1000 to 10000 simulations, as the precision depends on the number of simulations, given the dispersion shown in OV-PD/AP plots.

B. Case 2: Overvoltage control methods

Fig. 10 shows the statistical results for two OV control methods: 1) controlled switching and 2) surge arresters. Case 2 from Fig. 3 was used, with 1000 simulations, this was previously identified as sufficient for statistical analysis. Both techniques effectively limit OVs, narrowing their range compared to random switchings. Controlled switching achieves greater reduction of mean OV values and improves distribution spread. Maximum OVs during switching are shown in Fig. 11.

Reducing the time step to $\Delta t = 6.104\ \mu s$ has no significant impact on the simulations or statistical results. In contrast, time steps of 24.41 and $48.82\ \mu s$ introduced approximately 10% variations in maximum OV values, as it is shown in Fig. 11 for the $24.41\ \mu s$ case. This finding underscores the critical importance of selecting an appropriate time step to ensure accurate statistical analysis.

Fig. 12 compares the average computation times for each method across different simulation counts and highlights the average computation time per simulation for QMF-EMT. For the proposed method, its average computation time per simulation is 14.057 s. This includes 13.068 s for preprocessing and 0.9302 s for Kron's reduction, both are performed only once per simulation. The QMF-EMT computation time per simulation is 58.3 ms. As it is shown in Fig. 12, for 10000 simulations the QMF-EMT is 97 times faster than PSCAD/EMTDC and 51 times faster than the conventional NLT method. Notably, PSCAD/EMTDC simulations are initialized from a steady-state point to avoid full system compilation, the fastest possible execution at CPU level. It should be noted that PSCAD/EMTDC is a robust tool that supports various electrical studies. In contrast, the proposed tool is specifically designed for the studies presented in this article, resulting in significantly faster simulation times.

These results are specific to a three-phase switch, with simulation times scaling based on the number of nodes of interest analyzed.

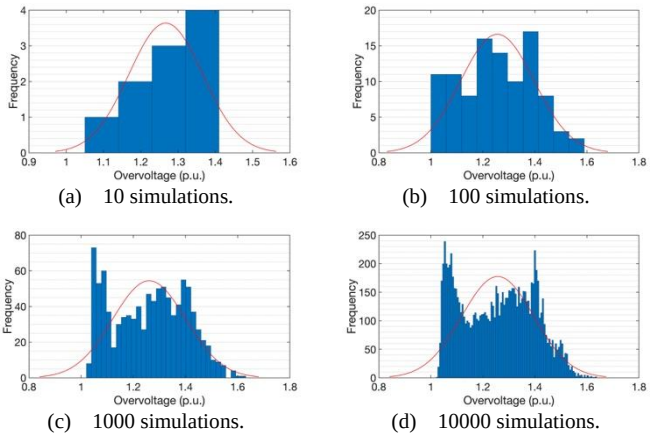

(a) 10 simulations. (b) 100 simulations. (c) 1000 simulations. (d) 10000 simulations.

Fig. 8. Probability distribution for openings at node *C*.

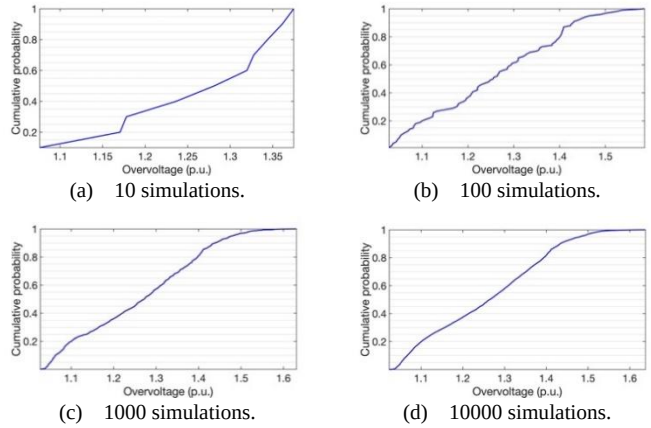

(a) 10 simulations. (b) 100 simulations. (c) 1000 simulations. (d) 10000 simulations.

Fig. 9. Cumulative probability for openings at node *C*.

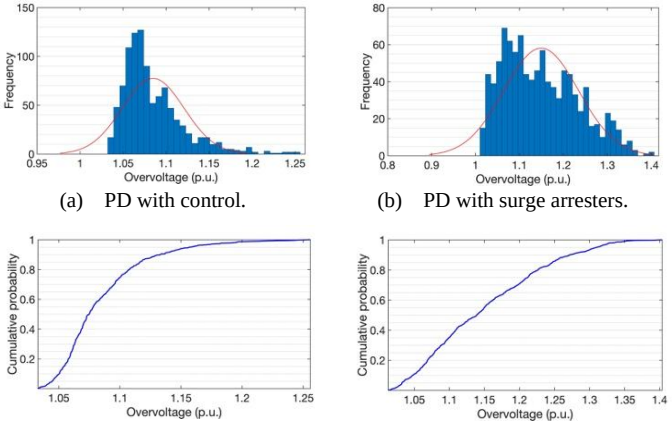

(a) PD with control. (b) PD with surge arresters. (c) AP with control. (d) AP with surge arresters.

Fig. 10. Statistical results with opening control and surge arresters (node *C*).

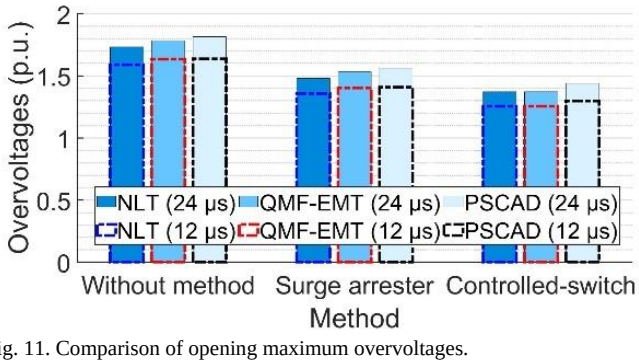

Fig. 11. Comparison of opening maximum overvoltages.

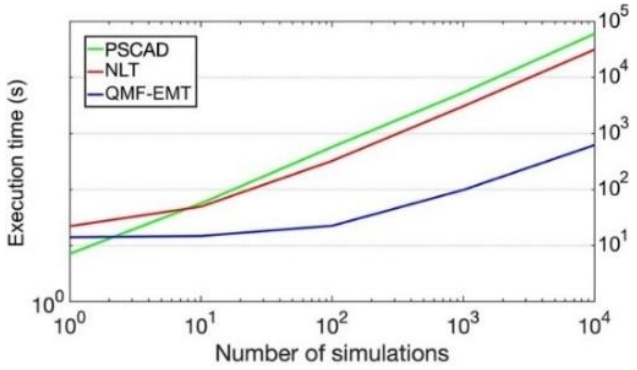

Fig. 12. Computational efficiency of simulation methods.

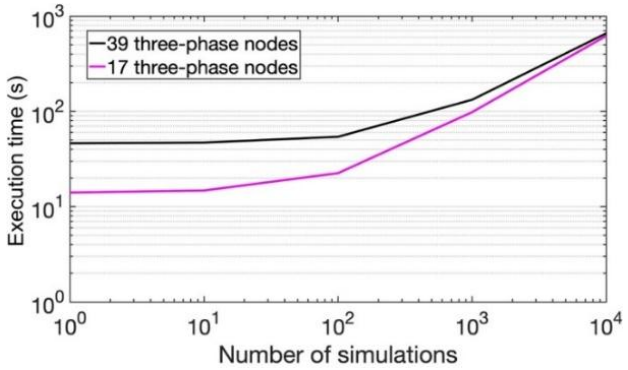

Fig. 14. Computational efficiency of QMF-EMT in the two test networks.

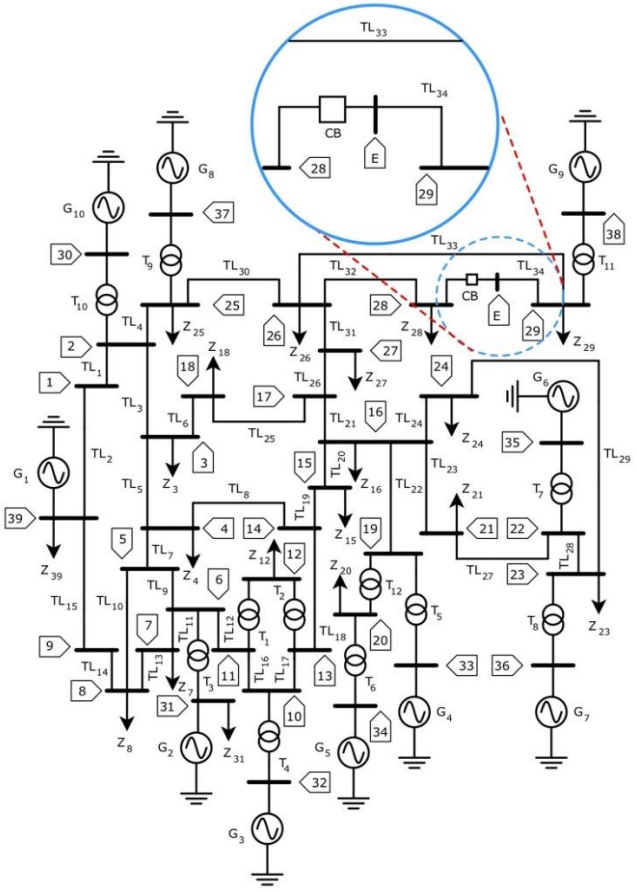

Fig. 13. One-line diagram of test network of 39 three-phase nodes.

TABLE II
CPU AVERAGE TIME OF QMF-EMT METHOD

CPU task	17 three-phase nodes case	39 three-phase nodes case
Preprocessing stage	13.068 *s*	37.186 *s*
Kron's reduction	0.9302 *s*	9.0353 *s*
1 simulation	0.0583 *s*	0.0585 *s*
10 simulations	0.7799 *s*	0.7807 *s*
100 simulations	8.4717 *s*	8.4814 *s*
1000 simulations	84.119 *s*	84.203 *s*
10000 simulations	605.13 *s*	605.31 *s*

VI. STATISTICAL STUDIES IN LARGE-SCALE POWER-SYSTEMS

To demonstrate the performance, scalability, and flexibility of the QMF-EMT method at SS, the 39-node, AC-60 Hz network in Fig. 13 is now used. The CB is placed between nodes 28 and E, with a closed switch resistance of $R_{sw} = 1\ m\Omega$.

The network parameters are detailed in [29], and the simulation parameters are the same as the previous statistical study. The AB frequency-dependent nodal matrices have been used for all the transmission lines. It is important to note that ideal voltage sources and non-magnetized transformer models are used in this application for all three simulation methods.

For this network, the same number of simulations was used to analyze various switching scenarios (from 10 to 10000 statistical simulations). As demonstrated earlier, the accuracy of SS depends on both, the number of simulations and the selected time step. Computational efficiency is compared with prior results in Fig. 14 and Table II.

Note in Table II that the average computation times with the QMF-EMT method are comparable to those in the previous statistical case for the 17 three-phase nodes network. The only notable difference is in the preprocessing stage, which increases due to the larger size of the test network.

This performance demonstrates a substantial reduction in analysis times for SS, enabling to perform 1000 simulations in just a few seconds and up to 10000 simulations in just a few minutes, even with high precision requirements—something difficult to achieve with conventional TD methods. Notably, the QMF-EMT method employed here does not rely on parallel computing. However, as documented in [26], simulation speeds could be accelerated by up to 1,843 times faster than real-time operation, excluding the preprocessing stage.

It should be noted that performing this amount of simulations with high precision using TD and FD tools on a conventional CPU, such as the one specified previously, is computationally intensive and very slow for the 17-node test network in the first statistical case, and this situation worsens for larger power-systems, such as the 39-node test network here analyzed.

VII. CONCLUSIONS

Statistical studies for insulation coordination typically involve thousands of EMT simulations, which traditionally require considerable computational time and cost. This article introduces QMF-EMT, a novel method that effectively addresses these challenges, enabling efficient and accurate

statistical analysis of transient behavior in electrical networks.

In QMF-EMT, the network model is synthesized in the frequency (Laplace) domain, thus avoiding the drawbacks of rational fitting techniques, such as non-passive models and network equivalents. Transient event simulations are performed in the TD using extensive convolutions and the superposition principle. In this way, undesirable aliasing effects, such as wind-around, are avoided. The proposed methodology is versatile and can accommodate nonlinear elements, such as surge arresters, as well as time-varying components, while maintaining precision and speed.

To validate the proposed method, transients from sequential switch operations in a 17-node three-phase network have been analyzed. Its accuracy and execution times have been benchmarked against PSCAD/EMTDC and the conventional NLT method, as in [3], [22]-[25], demonstrating its high performance. The efficiency of the proposed method has facilitated a statistical OV analysis with varying numbers of transient events, helping to determine the appropriate number of events for a specific study case. Additionally, a third application has incorporated surge arresters for OV control, while a fourth has extended the analysis to include controlled switch operations, offering comparative insights into OV mitigation strategies. It has also enabled the proper selection of the time step.

To demonstrate the scalability of the proposed method, it has been applied to the statistical EMT study of the IEEE-39 bus system, showing that high-precision simulations involving up to 10000 random events can be completed in seconds on a conventional CPU. In these cases, comparisons with PSCAD/EMTDC and the NLT method become impractical due to their excessive computational demands. For 10000 simulations, QMF-EMT was found to be 97 times faster than PSCAD/EMTDC and 51 times faster than the NLT method.

Notably, the increase in network size primarily affects preprocessing, as shown in Table II, while Fig. 14 demonstrates consistent execution times for a large simulation set. This highlights that QMF-EMT maintains computational efficiency regardless of network size. Furthermore, this outstanding performance was achieved without parallel computing. All implementations were executed on a conventional CPU within the Matlab environment.

VIII. ACKNOWLEDGMENT

This work was supported in part by the National Council of Science and Technology (CONACYT), Mexico, under Grant No. 1074592. The work of Luis A. Garcia-Reyes received funding from the ADOreD project, part of the European Union's Horizon Europe Research and Innovation Programme, under the Marie Skłodowska-Curie Grant Agreement No. 101073554.

IX. REFERENCES

[1] J. A. M. Velasco, *Coordinación de aislamiento en redes eléctricas de alta tensión*. McGraw Hill, 2013.

[2] P. Mestas and M. C. Tavares, "Relevant parameters in a statistical analysis-application to transmission-line energization," *IEEE Transactions on Power Delivery*, vol. 29, no. 6, pp. 2605–2613, 2014.

[3] P. Gómez and J. Segundo-Ramírez, "Frequency domain approach for statistical switching studies: Computational efficiency and effect of network equivalents," *Electric Power-systems Research*, vol. 196, pp. 107–257, 2021.

[4] D. Woodford and L. Wedepohl, "Transmission line energization with breaker pre-strike," in *IEEE WESCANEX 97 Communications, Power and Computing. Conference Proceedings*, 1997, pp. 105–108.

[5] J. Martinez, R. Natarajan, and E. Camm, "Comparison of statistical switching results using gaussian, uniform and systematic switching approaches," in *2000 Power Engineering Society Summer Meeting (Cat. No.00CH37134)*, vol. 2, 2000, pp. 884–889 vol. 2.

[6] H. W. Dommel, *EMTP theory book*. Boneville Power Administration, 1994.

[7] P. Gomez, "Validation of ATP transmission line models for a monte carlo study of switching transients," in *2007 39th North American Power Symposium*, 2007, pp. 124–129.

[8] H. Khalilnezhad, M. Popov, L. van der Sluis, J. A. Bos, and A. Ametani, "Statistical analysis of energization overvoltages in EHV hybrid OHL-cable systems," *IEEE Transactions on Power Delivery*, vol. 33, no. 6, pp. 2765–2775, 2018.

[9] M. L. J. Z. Fan Zhang, Xiongying Duan and Z. Liu, "Statistical analysis of switching overvoltages in UHV transmission lines with a controlled switching," *IET Generation, Transmission and Distribution*, vol. 13, 2019.

[10] S. Ghasemi, M. Allahbakhshi, B. Behdani, M. Tajdinian, and M. Popov, "Probabilistic analysis of switching transients due to vacuum circuit breaker operation on wind turbine step-up transformers," *Electric Power-systems Research*, vol. 182, p. 106204, 2020.

[11] M. Benesz, W. Nowak, W. Szpyra, and R. Tarko, "Application of statistical methods in insulation coordination of overhead power lines," in *2017 18th International Scientific Conference on Electric Power Engineering (EPE)*, 2017, pp. 1–4.

[12] A. Hamza, S. M. Ghania, A. M. Emam, and A. S. Shafy, "Failure risk analysis under switching surges in power transmission systems," *Electric Power-systems Research*, vol. 166, pp. 190–198, 2019.

[13] P. Gómez, "Performance evaluation of time domain transmission line models for a statistical study of switching overvoltages," *IEEE Latin America Transactions*, vol. 11, no. 4, pp. 1036–1046, 2013.

[14] Juan A. Martinez-Velasco, "Real-Time Simulation Technologies in Engineering," in Transient Analysis of Power-systems: Solution Techniques, Tools and Applications, IEEE, 2015, pp.72-99.

[15] B. Gustavsen and H. M. J. De Silva, "Inclusion of Rational Models in an Electromagnetic Transients Program: Y-Parameters, Z-Parameters, S-Parameters, Transfer Functions," in IEEE Transactions on Power Delivery, vol. 28, no. 2, pp. 1164-1174, 2013.

[16] M. Matar and R. Iravani, "A Modified Multiport Two-Layer Network Equivalent for the Analysis of Electromagnetic Transients," in IEEE Transactions on Power Delivery, vol. 25, no. 1, pp. 434-441, 2010.

[17] B. Gustavsen, Fast Passivity Enforcement for Pole-Residue Models by Perturbation of Residue Matrix Eigenvalues, IEEE Transactions on Power Delivery, Vol. 23 , No 4 , 2008.

[18] M. Matar and R. Iravani, "The reconfigurable-hardware real-time and faster-than-real-time simulator for the analysis of electromagnetic transients in power-systems," *IEEE Transactions on Power Delivery*, vol. 28, no. 2, pp. 619–627, 2013.

[19] XioRui Liu, Juan Ospina, Ioannis Zografopoulos, Alonzo Russel, and Charalambos Konstantinou. Faster than real-time simulation: Methods, tools, and applications. In Proceedings of the 9th Workshop on Modeling and Simulation of Cyber-Physical Energy Systems. Association for Computing Machinery, 2021.

[20] Venkata Dinavahi and Ning Lin. Parallel Dynamic and Transient Simulation of Large-Scale Power-systems. Springer, 2022.

[21] G. Lauss V. Jalili-Marandi P. Forsyth C. Dufour V. Dinavahi A. Monti P. Kotsampopoulos J. A. Martinez K. Strunz M. Saeedifard X. Wang D. Shearer M. Paolone. M. O. Faruque, T. Strasser. Real-time simulation technologies for power-systems design, testing, and analysis. Journal Articles of Electrical and Computer Engineering, pages 63–73, 2015.

[22] P. Moreno, P. Gomez, J. L. Naredo and J. Guardado, "Frequency domain transient analysis of electrical networks including non-linear conditions," *International Journal of Electrical Power and Energy Systems*, vol. 27, no. 2, pp. 139–146, 2005.

[23] N. Nagaoka and A. Ametani, "A development of a generalized frequency-domain transient program-FTP," in IEEE Transactions on Power Delivery, vol. 3, no. 4, pp. 1996-2004, Oct. 1988.

[24] P. Gomez and F. A. Uribe, "The numerical Laplace transform: An accurate technique for analyzing electromagnetic transients on power

system devices," *International Journal of Electrical Power and Energy Systems*, vol. 31, no. 2, pp. 116–123, 2009.
[25] P. Moreno, R. de la Rosa, and J. L. Naredo, "Frequency domain computation of transmission line closing transients," *IEEE Transactions on Power Delivery*, vol. 6, no. 1, pp. 275–281, 1991.
[26] J. Zuluaga, J. L. Naredo, L. Castanon, M. Vega, and O. Ramos-Leanos, "Parallel computation of power system EMTs through polyphase-QMF filter banks," *Electric Power-systems Research*, vol. 197, pp. 107–317, 2021.
[27] B. Filipovic-Grcic, I. Uglesic, S. Bojic, and A. Zupan, "Application of controlled switching for limitation of switching overvoltages on 400 kV transmission line," *International Conference on Power-systems Transients*, 2017.
[28] Damodar Valley Corp. Technical specification-electrical equipment. Available:https://india-re-navigator.com/utility/download/public/tender_uploads/tender-61fa322de4e43.pdf., 2017. Accessed: 2023-07-19.
[29] M. A. Pai, Energy Function Analysis for Power System Stability. Springer New York, 1989.